

1 **Elemental Stoichiometry of Particulate Organic Matter across the Atlantic Ocean**

2
3 Adam J. Fagan¹, Tatsuro Tanioka¹, Alyse A. Larkin¹, Jenna A. Lee¹, Nathan S. Garcia¹, & Adam
4 C. Martiny^{1,2,*}

5 ¹Department of Earth System Science, University of California, Irvine, CA, USA

6
7 ²Department of Ecology and Evolutionary Biology, University of California, Irvine, CA, USA

8 *Corresponding Author: amartiny@uci.edu

9
10 **Abstract:**

11 Recent studies show that stoichiometric elemental ratios of marine ecosystems are not static at
12 Redfield proportions but vary systematically between biomes. However, the wider Atlantic
13 Ocean is under-sampled for particulate organic matter (POM) elemental composition, especially
14 as it comes to phosphorus ([i.e., POP](#)). Thus, it is uncertain how environmental variation in this
15 region translates into shifts in C:N:P. To address this, we analyzed hydrography, genomics, and
16 POM concentrations from 877 stations on the meridional transects AMT28 and C13.5, spanning
17 the Atlantic Ocean. We observed nutrient-replete, high-latitude ecosystem C:N:P to be
18 significantly lower than the oligotrophic gyres. Latitudinal and zonal differences in elemental
19 stoichiometry were linked to overall nutrient supply as well as N vs. P [limitationstress](#). C:P and
20 N:P were generally higher in the P-stressed northern region compared to southern hemisphere
21 regions. We also detected a zonal difference linked to a westward deepening nutricline and a
22 shift from N to P [limitationstress](#). We also evaluated possible seasonal changes in C:N:P across
23 the basin and predicted these to be limited. Overall, this study confirms latitudinal shifts in
24 surface ocean POM ratios but reveals previously unrecognized hemisphere and zonal gradients.
25 This work demonstrates the importance of understanding how regional shifts in hydrography and
26 type of nutrient stress shape the coupling between Atlantic Ocean nutrient and carbon cycles.

29 **Plain language summary:**

30 Climate change is ~~anticipated~~predicted to influence the biological pump by altering
31 phytoplankton nutrient distribution. In our research, we conducted comprehensive measurements
32 of particulate matter concentrations during two large oceanographic field studies. We observed
33 systematic variations in organic matter concentrations and ratios across the Atlantic Ocean, both
34 latitudinally and longitudinally. Through statistical modeling, we determined that these
35 variations are associated with differences in the availability of essential nutrients for
36 phytoplankton growth. Our findings highlight the adaptive resource utilization among surface
37 ocean plankton, which in turn modulates the interplay between the ocean's nutrient and carbon
38 cycles.

39
40 **Key points:**

- 41 • There was systematic regional variation in POM concentrations and ratios across the
42 Atlantic Ocean.
- 43 • Latitudinal variability in C:N:P is linked to the nutrient supply rate and N vs. P
44 stresslimitation.
- 45 • Westward deepening isopycnals and nutricline and a shift from N to P stresslimitation
46 correspond to zonal variability in C:N:P
47

Formatted: Font: (Default) Tahoma

48
49
50
51
52
53
54
55
56
57
58
59
60
61
62
63
64
65
66
67
68
69
70
71
72
73
74
75
76
77
78
79
80
81
82
83
84
85
86
87
88
89
90
91
92
93

1. Introduction

The efficiency of the biological pump is anticipated to be affected by climate change through alteration in phytoplankton nutrient allocation and the C:N:P ratio (Galbraith + Martiny, 2015). Nevertheless, the influence of ocean warming on this efficiency is still uncertain, carrying potential repercussions for the ecosystems and global carbon cycle. Climate change is expected to impact the efficiency of the biological pump via changes in phytoplankton nutrient allocation and C:N:P. However, the impact of ocean warming on efficiency remains uncertain, with potential consequences for both ecosystems and the global carbon cycle (Kwon et al., 2022). Over the past few decades, studies have observed variability in marine plankton elemental composition and ecosystem elemental composition (Weber and Deutsch, 2010; Martiny et al., 2013b, a). Specifically, regions with nutrient-rich conditions have lower C:N:P ratios (equatorial, coastal, and temperate/polar regions), and nutrient-poor conditions (subtropical gyre regions) have higher ratios (Martiny et al., 2013b, a). However, data compilations include variations in both sampling and analytical methods (Martiny et al., 2014) as well as have limited spatial coverage. Therefore, large-scale sampling efforts like Bio-GO-SHIP are quantifying ecosystem particulate organic matter (POM) concentrations and their elemental ratios utilizing consistent methodology on a global scale (Tanioka et al., 2022; Clayton et al., 2022).

Studies focused on POM stoichiometry across ocean basins have been primarily limited to Bio-GO-SHIP cruises within the Indian Ocean (Garcia et al., 2018) and the Pacific Ocean (Lee et al., 2021). Both studies have observed high POM concentrations at higher latitudes and low concentrations within the gyres, with intermediate levels toward the equator. The stoichiometry had higher values in the gyres and lower values at high latitudes (Garcia et al., 2018; Lee et al., 2021). There have been two basin-wide transects across the Atlantic ocean that have been used in a global synthesis (Tanioka et al., 2022) but have not been used in a study focused solely on the Atlantic. Along with the strong relationship with latitude, there is also strong correlation with nutricline depth, used as a proxy for nutrient flux, in across each transect and the global synthesis, and so far, lack coverage for much of the Atlantic Ocean. Localized studies at the Bermuda Atlantic Time-series (BATS) site or short transects along the western North Atlantic Ocean show an N:P ratio between 40-50 and C:N near Redfield proportions (~6.6) (Michaels et al., 1994; Michaels and Knap, 1996; Steinberg et al., 2001; Babiker et al., 2004; Cavender-Bares et al., 2001). In contrast, POM dynamics and especially N:P and C:P ratios are less understood within the NE Atlantic Ocean and South Atlantic Ocean as a whole. Greater spatial coverage of POM measurements, both latitudinally and longitudinally, is needed to understand the coupled elemental cycles in the Atlantic Ocean.

The Atlantic Ocean has a unique dynamic, being singularly/co-limited by nitrogen and phosphorus respectively to the north of the equator and predominantly nitrogen limited south of the equator with phosphorus limitations north of and nitrogen limitations south of the equator (Cotner et al., 1997; Mather et al., 2008; Browning and Moore, 2023). In phosphorus co-limited regions, N:P and C:P are often elevated from frugal phosphorus use, supported by the well sampled NW Atlantic Ocean (Galbraith and Martiny, 2015; Lomas et al., 2010, 2022). In support, the well sampled NW Atlantic Ocean displays high N:P and C:P (Lomas et al., 2010, 2022). As a response to the nutrient limitation, phytoplankton can express

94 ~~specific genes that will allow for greater uptake of a nutrient. Gene expression and preferential~~
95 ~~uptake could influence cellular C:N:P within phytoplankton. Nitrogen~~ limitation is more
96 widespread in the South Atlantic Ocean, but no study has quantified ecosystem C:N:P here
97 (Mather et al., 2008; Ustick et al., 2021). ~~Temperature has been known to influence the~~
98 ~~concentration of cellular phosphorus in phytoplankton, with increasing in C:P with warmer~~
99 ~~temperatures, however C:N remains unchanged~~ (Yvon-Durocher et al., 2015). ~~The underlying~~
100 ~~mechanism for this relationship is not fully understood but hypothesized to be from either~~
101 ~~increase in carbon uptake over phosphorus, an increase in nutrient use efficiency, or (Tanioka~~
102 ~~and Matsumoto, 2020) translation compensation theory (few P-rich ribosomes are required for~~
103 ~~protein synthesis)~~ (Tanioka and Matsumoto, 2020). ~~The availability of nutrients generally follow~~
104 ~~inverse patterns of C:N:P, with increasing nutrients leading to a decrease in C:N and C:P and~~
105 ~~vice-versa~~ (Galbraith and Martiny, 2015; Tanioka and Matsumoto, 2017). ~~However,~~
106 ~~Temperature and other environmental factors are also important for C:N:P variability~~ (Yvon-
107 ~~Durocher et al., 2015), but how such environmental variation in~~ affects the Atlantic Ocean
108 elemental stoichiometry ~~remains largely~~ unknown. Therefore, the broad environmental
109 gradients in the Atlantic Ocean could result in significant regional ecosystem C:N:P shifts.

110 Here, we quantified suspended particulate organic carbon, nitrogen, and phosphorus
111 concentrations along two Bio-GO-SHIP meridional transects: AMT 28 and C13.5 (Fig. 1),
112 covering large parts of the Atlantic Ocean. We addressed ~~two~~ three questions: (1) What are
113 meridional, hemispheric, and zonal differences in POM concentrations and stoichiometry? And
114 (2) What is the relationship between environmental factors and C:N:P? We hypothesize that
115 differences in total nutrient supply and temperature are primarily responsible for the latitudinal
116 gradient in C:N:P. In contrast, the type of nutrient ~~stress~~ limitation will be important for
117 hemispheric and longitudinal C:N:P shifts.

118 2. Methods

119 2.1. Cruise Transects

120 AMT 28 started in Harwich, UK (49° 38' N/5° 30' W), and ended in Mare Harbour, Falkland
121 Islands (48° 12' S/52° 42' W), departing ~~the 25th~~ September ~~25,~~ 2018, and ending ~~the 27th~~
122 October ~~27,~~ 2018. C13.5 started in Cape Town, South Africa (34° 22' S/17° 18' W), and ended
123 in Norfolk, VA (36° 5' N/74° 34' W) (Fig. 1), departing ~~the 21st~~ March ~~21,~~ 2020, and ending
124 ~~the 16th~~ April ~~16,~~ 2020. C13.5 was set to go ~~45° S into the Southern Ocean~~ and collect samples
125 along the ~~e~~astern boundary of the South Atlantic Ocean. Due to COVID-19 quarantine
126 restrictions, it was redirected to a port in Virginia. Fortuitously, this redirect allowed sample
127 collection across the eastern South Atlantic Ocean and the western North Atlantic Ocean.

128 2.2. Sample ~~co~~Collection

129 Seawater for the POM was collected from the underway flow-through system for both cruises at
130 a depth of approximately 5 m. This method involved initially passing water through a 30 µm
131 nylon mesh to remove the stochastic presence of large particles from the samples (Lee et al.,
132 2021). We then collected ~~3 to 8~~ ~~L~~ liters of filtered water in 8.5 L plastic polycarbonate carboys
133 (Thermo Fisher Scientific, Waltham, MA). The carboys were placed at a 45° angle to prevent
134 particles from settling below the nozzle. Next, particulate organic carbon (POC), nitrogen
135 (PON), and phosphorus (POP) samples were filtered onto 25 mm pre-combusted GF/F (500°C
136 for 5 hours) (nominal pore size of 0.7 µm) (Whatman, Florham Park, NJ) (POC/PON ~~are~~ on the

Formatted: Font: (Default)Tahoma

Formatted: Font: (Default)Times New Roman

Formatted: Font: (Default)Times New Roman

Formatted: Font: (Default)Times New Roman

Formatted: Font: (Default)Times New Roman

Formatted: Font: (Default)Times New Roman

Formatted: Font: (Default)Times New Roman

Formatted: Font: (Default)Times New Roman

Formatted: Check spelling and grammar

141 same filter). POP filters were rinsed with 5 ml of 0.17 M Na₂SO₄ to remove traces of dissolved
142 phosphorous from the filter. Finally, we stored all filters in pre-combusted aluminum packets and
143 placed them in a -80°C freezer during the cruise, a -20°C cooler for shipping, and back to a
144 -80°C freezer until analysis. Between sample collections, the carboys and tubing were rinsed
145 with 30 µm filtered sample water just prior to collection.

146 We collected single samples of POC/PON and POP hourly for AMT₂₈. For the C13.5
147 transect, POC/PON and POP samples were collected in triplicate every ~~4 to 6~~ hours. Water
148 collection for C13.5 was done at the peak and trough of the diel cycle, ~06:00 and ~20:00 LT,
149 respectively, and with one to two a balance of collections in between those times. ~~to prevent bias~~
150 in sample collection.

152 2.3. Particulate organic matter determination

153 2.3.1. Particulate organic phosphorus (POP) assay

154
155 POP was analyzed using a modified ash-hydrolysis protocol (Lomas et al., 2010). Filters were
156 placed into acid-washed/pre-combusted glass vials with 2 ml of 0.017 M MgSO₄ and covered
157 with pre-combusted aluminum foil. The vials were placed in an incubator for 24 hours at 80 to -
158 90°C and then combusted for 2 hours at 500°C. After cooling, 5 ml of 0.2 M HCl was added
159 and incubated at 80 to -90°C for 30 minutes. The supernatant was collected, and the vials were
160 rinsed with 5 ml of Milli-Q water. The rinse water was collected and added to the supernatant. 1
161 ml of mixed reagent (2:5:1:2 parts ammonium molybdate tetrahydrate (24.3 mM), sulfuric acid
162 (5 N), potassium antimonyl tartrate (4.1 mM), and ascorbic acid (0.3 M) was added to the
163 supernatant and left in the dark for 30 minutes. Samples were analyzed on a spectrophotometer at
164 a wavelength of 885 nm using a potassium monobasic phosphate standard (1.0 mM-P). The
165 detection limit for POP measurements was ~0.3 µg.

167 2.3.2. Particulate organic carbon/nitrogen (POC/PON) assay

168
169 POC/PON are measured using the same filter. The POC/PON samples were processed in the lab
170 at UCI using a JGOFS protocol (Ducklow and Dickson, 1994). POC/PON samples were dried in
171 an incubator at 55°C for 24 hours. They were then moved to a desiccator with concentrated
172 HCl fumes for 24 hours to remove inorganic carbon. The samples were then re-dried at 55°C
173 for 24 hours before being packaged into pre-combusted tin capsules (CE Elantech, Lakewood,
174 NJ). The packaged filters were analyzed on a CN FlashEA 1112 Elemental Analyzer (Thermo
175 Scientific, Waltham, MA) with atropine and acetanilide standards. POC and PON measurements
176 had a detection limit of ~2.4 µg and ~3.0 µg. Settings for the FlashEA had an oxidative reactor
177 temperature of 900°C, a reduction reactor temperature of 680°C, and an oven temperature of
178 50°C. Oxygen introduced to the oxidative reactor last seven seconds allowing temperatures to
179 reach 1800°C for sample combustion. A leak test needed to fall below 5 ml min⁻¹ before
180 samples were analyzed to minimize sample loss.

182 2.4. Nutrient availability, bio geography, and biological properties

183 2.4.1. Nutricline depth

184
185 The nutricline depth was determined as the 1 µM nitrate depth horizon (Garcia et al., 2018;
186 Cermeño et al., 2008). Nutricline depth was regarded as a proxy for nutrient supply to the

187 surface, with a shallow nutricline representing a high flux of nutrients and vice-versa for a deep
188 nutricline. The nutricline depth with respect to the 1/16 μM phosphate depth horizon was also
189 investigated but found to be nearly identical to that of nitrate. For AMT28, nitrate concentrations
190 were quantified as previously described from CTD casts along the transect (Swift, 2019). Nitrate
191 concentrations were then interpolated using DIVA implemented in Ocean Data View (v5.5.2)
192 (Schlitzer, 2019). For C13.5, we used the seasonal average nitrate depth profiles from 2018 of
193 the World Ocean Atlas at one 1-degree spatial resolution to determine nutricline depths. This
194 approach was necessary as the logistical issues related to COVID quarantine restrictions
195 prevented us from collecting onboard CTD measurements. Linear interpolation for each profile
196 within the one 1-degree was performed to estimate the nutricline depth.

197 198 2.4.2. Delineation of Regions

199
200 The regions under consideration for this study are the Eastern Temperate North Atlantic
201 Subpolar (ETNASP) [Lat. 49.6°N-43.2°N] Western North Atlantic Gyre (WNAG) [Lat. 34.5°N-
202 19.8°N], Eastern North Atlantic Gyre (ENAG) [Lat. 43.0°N-18.1°N], Western Equatorial (WEQ)
203 [Lat. 17.9°N-5.9°S], Eastern Equatorial (EEQ) [Lat. 17.8°N-5.9°S], Western South Atlantic Gyre
204 (WSAG) [Lat. 6.0°S-34.0°S], Eastern South Atlantic Gyre (ESAG) [Lat. 6.2°S-33.0°S], Western
205 Temperate South Atlantic-Southern Ocean (WTSASO) [Lat. 34.1°S-48.2°S], and Eastern
206 Temperate South Atlantic-Southern Ocean (ETSASO) [Lat. 33.9°S-41.5°S] (Fig. 1). These
207 boundaries are determined using inflection points along the nutricline depth and the temperature
208 profile.

209 210 2.4.3. Cell Size

211
212 Cell size was determined by the conversion of cell count based on flow cytometry samples
213 collected during CTD casts (AMT28) at the top 200 m of the water column. (Moreno et al.,
214 2022). Flow cytometry samples (63 stations, 755 samples) were co-collected with the POM
215 samples used in this study. Cell count was determined using two methodologies. The first
216 method was collected without a filter and utilized an inverted microscope to estimate cell
217 abundance and phytoplankton species composition (Utermöhl, 1958). This allowed for the
218 estimates of diatoms, dinoflagellates, and coccolithophores. The second method measured cells
219 using a Becton Dickinson FACSort flow cytometer to measure *Prochlorococcus*, *Synechococcus*,
220 and pico-eukaryotes. Combining these two methods of collection allowed for a complete survey
221 of phytoplankton groups.

222 Conversion of cell count to biomass (fg C/cell) was done following the methodology
223 from Moreno et al., 2022. Briefly, pPhotoautotrophs were categorized into *Prochlorococcus*,
224 *Synechococcus*, pico-eukaryotes, nano-eukaryotes, *Coccolithophore*, and *Cryptophytes*. Each cell
225 type had a specific conversion factor in determining its biomass. Using a Monte Carlo approach,
226 95% confidence interval around cell size was determined using a normal distribution based on
227 the mean and standard deviation. Then, a randomly chosen conversion factor was applied to each
228 type. Allowing for 1000 runs, we estimate a 95% confidence interval (Moreno et al.,
229 2022).(Moreno et al., 2022).

230 231 2.4.4. Metagenomics-~~i~~nformed nNutrient stress~~Limitation~~

Formatted: Indent: First line: 0.5"

233 Metagenomically informed nutrient stress utilizes a subset of data from Ustiek et al., 2021,
234 utilizing the genome content of *Prochlorococcus* from the Atlantic Ocean. Element specific
235 nutrient stress was based on the global genome content of *Prochlorococcus* (Ustiek et al., 2021).
236 These metagenomic samples (276) were co-collected with the POM samples, across both
237 transects, used in this study. Based on variation in *Prochlorococcus* population gene content, this
238 study identified genes associated with nitrogen and phosphorus nutrient stress types. The severity
239 of nutrient stress was quantified by calculating the frequency of nutrient acquisition genes within
240 *Prochlorococcus* single-copy core genes and attributes the frequency to the genetic adaptation
241 for overcoming nutrient stress type and severity. Moving forward the use of nitrogen/phosphorus
242 gene index will refer to this calculation of the high-nutrient stress. Although based on
243 *Prochlorococcus*, there is a significant overlap between this genetic index of nutrient stress and
244 both Earth System Models and whole community nutrient addition assays (Ustiek et al., 2021).
245 Ustiek et al., 2021 associated *Prochlorococcus* gene expression occurrences with different
246 environmental nutrient stress conditions. They separated the genes by nutrient type (nitrogen,
247 phosphorus, and iron) and nutrient stress severity (low, medium, and high). Our study utilizes the
248 high stress severity for nitrogen and phosphorus. Iron has a more indirect influence on the C:N:P,
249 than nitrogen and phosphorus, which is why it will be omitted from this study. The stress
250 severity associated with medium or low stress either followed the same pattern as the high
251 nutrient stress or had no pattern at all, respectively, which is why this is also omitted. The
252 function of the genes associated with high gene index are *focA*, *moaA-E*, *moeA*, *napA*, *narB*, *nirA*
253 (for nitrogen) and *phoA*, *phoX* (for phosphorus). The functions of these genes are for the
254 assimilation and uptake of nitrite and nitrate, and production of alkaline phosphatase.
255 The described metagenomic samples (276) were co-collected with the POM samples used in this
256 study. Based on variation in *Prochlorococcus* population gene content, we identified genes
257 associated with N and P nutrient stress types. Briefly, gene index, or the severity of the nutrient
258 stress, is quantified by calculating the frequency of nutrient acquisition genes within
259 *Prochlorococcus* single-copy core genes and attributes the frequency to the genetic adaptation
260 for overcoming nutrient stress type and severity. Although based on *Prochlorococcus*, there is a
261 significant overlap between this genetic index of nutrient limitation and both Earth System
262 Models and whole community nutrient addition assays (Ustiek et al., 2021). Of the different
263 intensities and types of stress, our study utilized data with gene information representing the
264 most severe form of nutrient gene index for nitrogen and phosphorus stress.

265 2.4.5 N* Derivation

266 The derivation from Redfield nutrient concentration (N*) at a depth of 200 m was calculation:

$$267 \quad N^*_{200} = [\text{NO}_3]^{-1}_{200} - 16[\text{PO}_4]^{-3}_{200}$$

271 A negative/ declining value would be indicative of nitrogen stress, while a positive/ increasing
272 value would indicate phosphorus stress.

273 2.5. Data Analysis

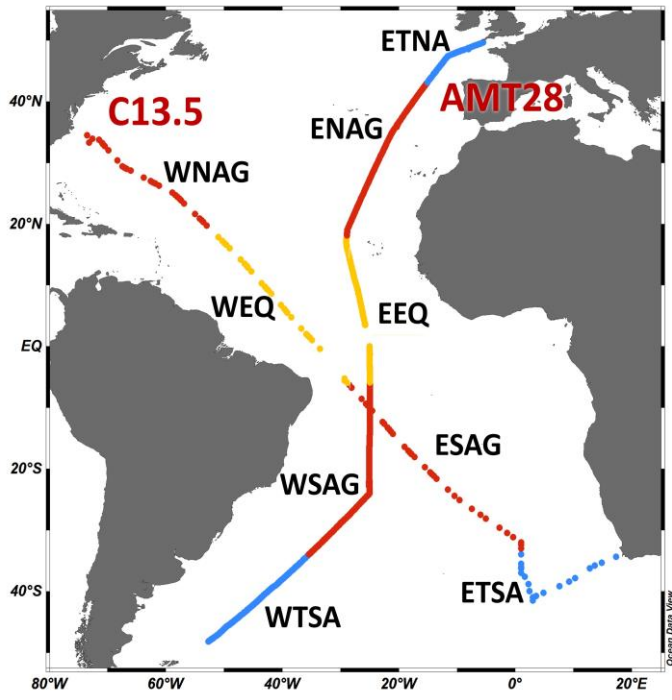
274 Data analysis was conducted using Matlab R2021b (MathWorks). An ANOVA analysis with a
275 posthoc Tukey test was used to determine the relationship between the selected regions for
276

Formatted: Font: Italic

Formatted: Font: Not Italic

279 environmental conditions and POM. The C:N:P ratios underwent a log transformation to achieve
280 a normal distribution before the ANOVA analysis (Isles, 2020). Using R ver. 4.1.2 (R Core
281 Team, 2021), we used generalized additive models (GAM) with package *mgcv* (v1.8) (Wood,
282 2017) to explain the strength of four variables in determining C:N:P (temperature, nutricline
283 depth, nitrogen [gene indexstress](#), and phosphorus [gene indexstress](#)).
284

285 **3. Results**

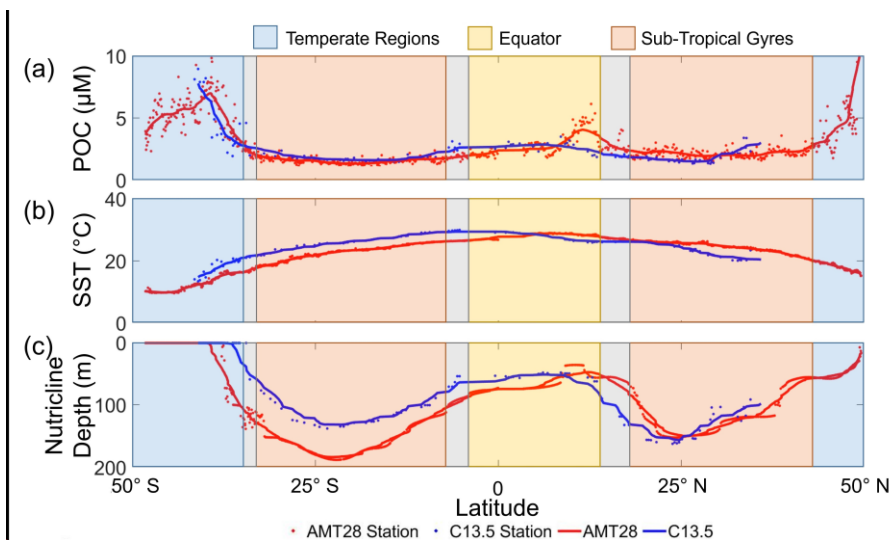


Formatted: Font: Times New Roman
Formatted: Centered

286 **Figure 1.** Map of oceanographic cruise transects AMT 28 (September 25 to October 27, 2018, n = 765) and C13.5
287 (March 21 to April 16, 2020, n = 112). Different oceanographic regions are separated using nutricline and
288 temperature profiles (WTSA = Western Temperate South Atlantic, ETSA = Eastern Temperate South Atlantic,
289 WSAG = Western South Atlantic Gyre, ESAG = Eastern South Atlantic Gyre, WEQ = Western Equatorial, EEQ =
290 Eastern Equatorial, WNAG = Western North Atlantic Gyre, ENAG = Eastern North Atlantic Gyre, ETNA = Eastern
291 Temperate North Atlantic). Colors delineate temperate (blue), subtropical (red), and equatorial upwelling regions
292 (yellow).
293
294
295

296 POM concentrations, temperature, and nutricline profiles exhibited unique characteristics to
297 each oceanographic region. Between the two transects, POC, PON, and POP concentrations were
298 strongly/moderately correlated ($r = 0.6845, 0.7148, \text{ and } 0.7049$, respectively; $p < 0.001$) and
299 showed overall similar biogeography (Fig. 2aA and S1). All POM pools had peak concentrations
300 at high latitudes, troughs in the subtropical gyres, and intermediate concentrations at the equator.
301 In high latitude temperate/subpolar regions (WTSA, ETSA, and ETNA), POC (and
302 overall POM) was significantly elevated (4.6 to 5.3 μM ; $p < 0.05$) compared to all other regions
303 (Equatorial: 2.8 μM , Gyre: 1.6 to 2.1 μM) (Fig. 2aA, Fig. S2). POM concentrations also
304 showed a zonal difference. There were higher concentrations of POM in the western regions
305 compared to the eastern region of the Temperate South Atlantic/Southern Ocean, whereas the
306 opposite was seen in the subtropical gyres (Fig. 2aA and Fig. S2). At $\sim 10^\circ \text{S}$, C13.5 and AMT_28
307 cross paths; we used a 1° cell centered on the intersection (using 9 samples), to find the

308 difference between the POC, PON, and POP of the two cruises was 0.2%, 5.7%, and 10.6%
 309 respectively, indicating that seasonal variability between the had the greatest impact on POP,
 310 within this cell. However, one sample is the cause of most of the error, within PON and POP,
 311 removing the sample the difference becomes 2.9%, and 2.1% respectively. We observed nearly
 312 identical POM concentrations (and ratios), suggesting a stable POM level despite sampling in
 313 different seasons. Temperature peaked equatorially ($\sim 28^{\circ}\text{C}$) for both transects and declined
 314 with increasing latitudes (Fig. 2**B**). We observed minor variation in the meridional temperature
 315 profile linked to the difference in the seasonal timing for each cruise leading to a slight
 316 southward shift in peak temperature during C13.5. Nutricline profiles for both transects were
 317 similar, with the deepest nutricline in the gyres and shallowest at high latitudes and the equator
 318 (Fig. 2**C**). Zonal variability in the nutricline depth was apparent, with the deepest values in the
 319 western side (135 to– 150 m) compared to the eastern side of the gyres (114 to– 116 m) (Fig.
 320 S2). Thus, we observed a robust meridional gradient in POM concentrations and environmental
 321 conditions but also a zonal gradient in nutricline depth in the oligotrophic subtropical gyres.
 322
 323



324 **Figure 2.** Meridional variability in POC concentrations and environmental conditions for AMT28 (boreal fall) and
 325 C13.5 (boreal spring). (a) Averaged surface POC concentrations, (b) surface temperature, and (c) nutricline depth
 326 presented as $Z_{\text{nutrate}} > 1 \mu\text{M}$. The trend lines represent the moving average of samples for AMT28 (red/ $n=50$) and
 327 C13.5 (blue/ $n=20$) transects. Background colors indicate broad oceanographic regions separated by latitude (blue =
 328 Temperate, red = Subtropical, yellow = Equatorial upwelling regions). Grey spaces between regions represent the
 329 difference in boundaries between the two transects.
 330

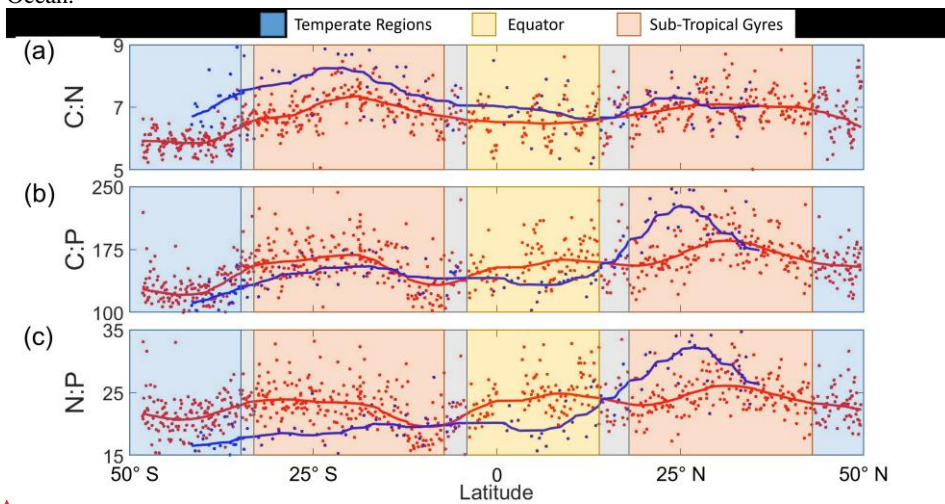
331
 332 We observed distinct latitudinal, zonal, and hemispheric C:N:P variability (Fig. 3). First,
 333 we detected peak ratios in the subtropical gyres, troughs in the high latitudes, and intermediate
 334 values at the equator for C:N, C:P, and N:P, matching patterns seen globally (Martiny et al.,
 335 2013b) (Martiny, Pham et al., 2013). In the subtropical gyres, averaged C:N values were
 336 noticeably elevated (7.0 to– 7.6) compared to the other regions (TemperateSub-Polar: 6.0 to–7.2,

Formatted: Indent: First line: 0"

Formatted: Font: Times New Roman

Formatted: Centered

337 EQ: 6.6 to 6.8) (Fig. 3aA). C:P followed the same trend as C:N, with subtropical gyre regions
 338 being higher (148 to 208) than the other regions (TemperateSub-Polar: 122 to 158, EQ: 136
 339 to 161) (Fig. 3bB). N:P showed parallel changes to C:P except the South Atlantic Gyre
 340 showing a N:P range encompassing those of all other regions (20.1 to 29.2) (Fig. 3cC).
 341 Second, a zonal gradient was detected, whereby C:N was higher in the eastern side of the
 342 South Atlantic Ocean compared to the western side South Atlantic Ocean (Fig. 3D).
 343 However, this zonal gradient was not observed seen in other regions. C:P also showed an
 344 opposite zonal trend with higher values on the western side, albeit only significantly different in
 345 the northern hemisphere (Fig. 3eE). N:P showed the highest zonal variation. This ratio was
 346 significantly higher on the western side (21.4) compared to the eastern side (17.1) side of the
 347 South Atlantic Subtropical Gyre (Fig. 3fF), converging at ~10° S and again elevated on the
 348 western side (29.2) compared to the eastern sidepart (24.8) of the North Atlantic Subtropical
 349 Gyre (Fig. 3fF). Again, using the 1° cell centered on this intersection, we determined C:N, C:P,
 350 and N:P had a 5.8%, 12.1%, and 5.9% difference, respectively, between the two cruises. One
 351 sample is the cause of a majority of the error, with its removal the difference becomes 2.6% for
 352 C:N and 1% for the rest. Third, there was also a hemisphere bias, whereby C:P, and N:P were
 353 elevated in the northern hemisphere and C:N somewhat higher in the southern hemisphere. In
 354 summary, we saw clear latitudinal, zonal, and hemisphere gradients in C:N:P across the Atlantic
 355 Ocean.



Formatted: Font: Times New Roman

395 of stoichiometry using a general additive model (GAM) (Fig. 4). Using flow cytometry cell
396 counts, we were able to determine the concentration and total biomass of separate species of
397 photoautotrophs at each station for AMT28. From this, *Prochlorococcus* was determined to
398 make up >93% of the community in the subtropical gyres and equator, and over 50% of the total
399 biomass. 67% of the northern sub-polar region community consisted of *Prochlorococcus* but
400 only 10% of the biomass, and the Southern Ocean was the only region without *Prochlorococcus*
401 being the most abundant at 12% of the community and 1% of the biomass (Fig. S4). The
402 variation in phytoplankton composition correlated significantly, but weakly, to shifts in
403 elemental composition ($r = 0.23$ $p < 0.05$). However, shifts in phytoplankton biodiversity did
404 only replicate the overall latitudinal shifts in C:P but failed to capture the detailed transitions
405 (Fig. S5). Thus, it was unclear how strongly shifting biodiversity impacted the elemental
406 stoichiometry.

407 A general additive model (GAM) with temperature and various dimensions of nutrient
408 availability. Using GAM, we determined temperature and the nutrient gene indices captured
409 67% and 56% of the total deviance for C:P and N:P, respectively. For C:P, nutrient depth and
410 phosphorus gene index stress accounted for 52.53% of the total (31.3% and 21.2%, respectively).
411 For N:P, nutrient depth and phosphorus gene index stress accounted for 45% of the total
412 (24.65% and 20.74%, respectively). We could only explain 30% less of the total deviance for C:N
413 (30%), with the temperature being the most significant contributors (13% and 11%, $p < 0.001$
414 and $p < 0.01$ respectively). For C:N:P, nutrient depth was the dominant contributor to the
415 latitudinal variability for two of the three ratios, being the second most dominant in the third,
416 when investigating the entire basin (Fig. 4). When dividing the Atlantic Ocean into eastern and
417 western boundaries, the four drivers tested were able to explain the variability of C:P and N:P
418 more accurately in the western side (81% and 63% respectively) and C:P in the eastern side
419 (38%) (Fig. S7 and S8, Table S2). From this division the dominant drivers remained nutrient
420 depth and temperature for C:P and N:P, and became the dominant driver of C:N. While the
421 drivers for C:N individually have a maximum of 7% difference between each other on either side
422 of the Atlantic Ocean, regional focus is able to interpret changes in drivers that an ocean wide
423 analysis would determine to be different. As both temperature and nutrient depth were strongly
424 correlated with latitude, these two factors also explained the majority of the latitudinal variability
425 of C:N:P. The remaining percentage that would explain the variation of stoichiometry may be
426 factors not taken into consideration for this study. Nevertheless, a combination of temperature
427 and nutrient stress described most of the stoichiometric variability in the Atlantic Ocean.
428

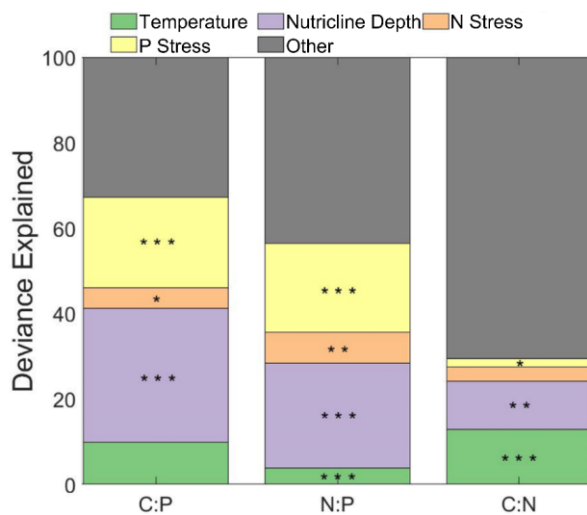
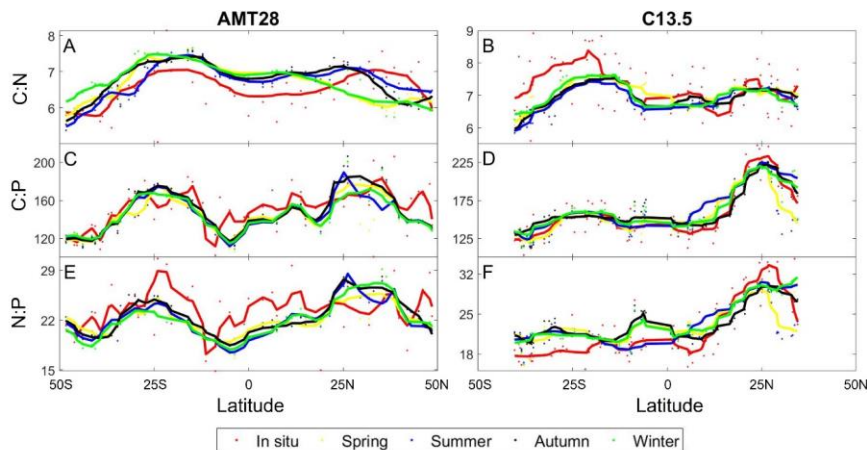


Figure 4. Influence of environmental factors on stoichiometry. Stars indicate the significance of smooth terms used for Generalized Additive Models (GAM). *** = $p < 0.001$, ** = $p < 0.01$, * = $p < 0.05$. Green represents the influence of temperature, purple represents the influence of nutricline depth, orange represents the nitrogen stress, yellow represents the phosphorus stress, and grey represents the remaining factors of influence on the variability of C:N:P. N and P stress are reflective of the nutrient gene index, which is quantified by calculating the frequency of the nutrient acquisition genes within *Prochlorococcus* single-copy core genes. The frequency is attributed to the genetic adaptation for overcoming nutrient stress type and severity.

A zonal gradient in nutricline depth and metagenomically-assessed nitrogen and phosphorus stress (gene index)-matched C:N:P shifts (Fig. 3d-f). Nutricline depth was significantly deeper ($p < 0.05$) in the western part of subtropical gyres in both hemispheres (Fig. S2). Furthermore, there was a westward shift from nitrogen towards phosphorus stress limitation (Fig. S6). This zonal shift in nutrient availability corresponds to a similar increase in C:P from 174 to 207 and N:P from 24.8 to 29.2 towards the western side of the oligotrophic gyres (Fig. 3e, f). In parallel, C:N showed the opposite trend declining from 7.6 on the eastern to 7.0 on the western side, matching a shift from nitrogen to phosphorus stress (Fig. 3D). GAM analyses conducted separately for western and eastern basins corroborated these observations highlighting that the relative importance of nitrogen vs. phosphorus shifting nutrient stress (Fig. S7-9). In summary, zonal variability in nutrient stress, described by a westward deepening nutricline and increased phosphorus P-gene index stress, may regulate a zonal change in C:N:P.

Formatted: Font: Times New Roman

Formatted: Font: 10 pt



452 **Figure 5.** Predicted seasonal variability of stoichiometry across the Atlantic Ocean. Observed compared to predicted
 453 seasonal C:N for AMT28 (A) and C13.5 (B). Observed compared to predicted seasonal C:P for AMT28 (C) and
 454 C13.5 (D). Observed compared to predicted seasonal N:P for AMT28 (E) and C13.5 (F). Dots are discrete samples
 455 and the lines are moving averages over ten samples. AMT28 occurred during the fall 2018 and C13.5 during the
 456 spring 2020. In situ samples are red, predicted Spring is yellow, predicted Summer is blue, predicted Autumn is
 457 black, and predicted Winter is green.

459
 460 We assessed the potential impact of seasonal environmental changes for C:N:P across the
 461 Atlantic Ocean. Seasonal environmental changes were characterized as shifts in nutricline depth
 462 and temperature, while assuming a stable biogeography of **nitrogen** vs. **phosphorus** stress
 463 (Fig. 5). This assumption is the result of only having gene stress information from the season
 464 samples were collected in. As a control, we saw a significant correlation between the observed
 465 and predicted C:N:P for the season matching the cruise occurrence (Table S3). However, the
 466 statistical model did not predict high C:N in the eastern South Atlantic Ocean and overestimated
 467 N:P in the equatorial and western South Atlantic Ocean. C:N:P ratios were predicted to be
 468 mostly stable across seasons. Although we detected shifts in C:N near the **north** sub-tropical
 469 convergence zone ($\sim 18^{\circ}\text{C}$) reflecting an expansion and contraction of oligotrophic conditions
 470 (Fig. 5aA). The introduction of more dynamic biogeography of nutrient stress will be necessary
 471 to predict a more accurate seasonal variability of C:N:P across the Atlantic Ocean. However,
 472 from data available our statistical model predicted a mostly stable, seasonal C:N:P across the
 473 Atlantic Ocean. However, C:P and N:P were predicted to be mostly stable. When assuming a
 474 stable biogeography of N and P stress zone, our statistical model predicted a mostly seasonally
 475 stable C:N:P across most of the Atlantic Ocean.

476 4. Discussion

477
 478
 479 There was clear latitudinal variability in POM concentrations and stoichiometry across the
 480 Atlantic Ocean. We detected a high POM concentration and low C:N:P at higher latitudes, low
 481 POM concentrations and high ratios in the subtropical gyres, and intermediate values near the
 482 equator. This meridional gradient in POM concentrations and ratios corresponded to parallel
 483 changes in nutricline depth and thus likely linked to the overall nutrient supply. Similar gradients

Formatted: Font: Times New Roman

Formatted: Indent: First line: 0.25"

484 in concentrations and ratios have been detected in the Indian Ocean (Garcia et al., 2018), the
485 Pacific Ocean (Lee et al., 2021), and in ~~a~~ a global synthesis (Martiny et al., 2013b). Thus, our
486 ~~new~~ observations add further support to systematic biome shifts in C:N:P across major ocean
487 basins. Despite having similar gradients, the North Atlantic Ocean appears to be relatively
488 unique with higher C:P and N:P ratios in the northern hemisphere compared to the south. Both
489 the North Atlantic and the Indian Ocean's Bay of Bengal ~~both~~ have comparable aerolian iron
490 inputs, however, North Atlantic Ocean has an increase in N₂-fixation, which increases the N:P
491 nutrient supply ratio, leading to widespread phosphorus stress (Capone, 2014; Schlosser et al.,
492 2014; Ussher et al., 2013). The Bay of Bengal does not have significant N₂-fixation nor a
493 significant change in C:P or N:P ratios (Garcia et al., 2018; Löscher et al., 2020). This lack of
494 N₂-fixation is possibly the result of stress from another micronutrient for N₂-fixers.

495 _____ Focusing on the influence of High aeolian iron input to the North Atlantic Ocean supports
496 the growth of nitrogen fixers, increases the N:P nutrient supply ratio, and causes widespread P
497 stress (Capone, 2014; Schlosser et al., 2014; Ussher et al., 2013). (Löscher et al., 2020) Such
498 phosphorus P gene index P stress stress, there is an likely impacts the observed increase in
499 phytoplankton elemental higher C:P and, to a lesser extent, N:P throughout much of the North
500 Atlantic Ocean. POP has a minimum concentration in the western North Atlantic Ocean (Fig.
501 S1), suggesting that the parallel changes in N:P and C:P are caused by lower POP
502 concentrations. Iron inputs decrease across the North Atlantic Ocean from east to west, with a
503 majority of the POP concentrations following the same trend (Mahowald et al., 2005). While
504 there is an increase in POP concentrations for C13.5, part of this is attributed to coastal
505 upwelling. Had C13.5 continued North it is possible that the POP concentrations observed in the
506 lower half of the North Atlantic gyre would have continued. Proposed explanations of this zonal
507 difference results from a combination of vertical iron supply and lateral circulation across the
508 Atlantic Ocean (Martiny et al., 2019). In the South Atlantic Ocean, aeolian iron inputs are
509 significantly lower, as most iron dust is washed out at the Intertropical Convergence Zone
510 (Capone, 2014). N₂-nitrogen fixation is hence suppressed (Wang et al., 2019), allowing most of
511 the southern hemisphere to have apart to be partially nitrogen gene index display elevated N
512 stress limited. This rise in the nitrogen N gene index stress limitation likely causes the depressed
513 PON concentrations (Fig. S1) and elevated C:N but depressed N:P in much of the South Atlantic
514 Ocean. Thus, the hemisphere deviation in C:N:P is hypothesized to be driven by a causal link
515 between iron inputs, N₂-fixation, and shifts between the nitrogen N and phosphorus P gene
516 index limitation (Martiny et al., 2019).

517 _____ An additional zonal gradient in C:N:P may be linked to the westward deepening of the
518 nutricline and a parallel shift from primarily nitrogen N stress towards an increase in phosphorus
519 P stress limitation. Phosphorus P stress limitation is detected throughout the central North
520 Atlantic Ocean based on both the gene index and N* (Ustick et al., 2021), however ~~but~~ both C:P
521 and N:P are significantly higher on the western side. Using the nutricline depth as proxy of
522 nutrient supply, the nutrient supply flux appeared greater on the eastern side. ~~In~~ addition,
523 aeolian nutrient inputs could relieve nutrient stress towards the east, suppressing C:P and N:P
524 ratios (Kremling and Streu, 1993; Mills et al., 2004; Garcia et al., 2018; Neuer et al., 2004). The
525 South Atlantic Ocean also has the east-west variability for C:N:P, ~~although C:N having the~~
526 largest gradient the gradient is highest for C:N. From the nutrient gene index and N*, the South
527 Atlantic Ocean is predominantly nitrogen stressed. ~~These~~ zonal shifts in C:N:P can be
528 explained by shallower nutricline depth and a higher stronger nitrogen N gene index limitation in
529

Formatted: Font: Font color: Black

Formatted: Indent: First line: 0"

530 the eastern part and ~~higher~~~~stronger~~ phosphorus P gene index ~~limitation~~ in the western part of the
531 South Atlantic Ocean (Ustick et al., 2021); (Martiny et al., 2019). Thus, we observe ~~important~~
532 zonal variability in POM concentrations and their stoichiometric ratios, superimposed on the
533 larger meridional and hemisphere gradients.

534 Nitrogen and phosphorus stress are assessed based on genomic changes and adaptation in
535 *Prochlorococcus* populations (Ustick et al., 2021). With *Prochlorococcus* being the most
536 abundant phytoplankton and that it forms most of the phytoplankton biomass in the gyres and
537 equatorial regions, and northern temperate population, it ~~would likely be~~ likely closely linked
538 to ~~representative of~~ the bulk phytoplankton community physiological status (Fig. S4) (Marañón
539 et al., 2000; Zwirgmaier et al., 2007). Additionally, *Prochlorococcus* and *Synechococcus*
540 express ~~nearly the same~~ identical gene responses across a transect with regions of different
541 nutrient stress (i.e. when *Prochlorococcus* had a high phosphorus gene index, *Synechococcus*
542 had a high phosphorus gene index as well) (Garcia et al., 2020). Within the South Atlantic
543 Ocean, the use of bioassays and deficiency calculations agree with *Prochlorococcus* gene stress,
544 being primarily nitrogen stressed, yet disagree within the North Atlantic Ocean (Browning and
545 Moore, 2023). While previous ~~bottle experiments~~ assessments of nutrient stress in the North
546 Atlantic Ocean describe it as being dominantly or co-stressed by nitrogen and phosphorus,
547 respectively, the gene index describes the North Atlantic as dominantly phosphorus stressed.
548 This suggests that there is a significant difference between the different ~~bio~~assays in determining
549 the nutrient stresses phytoplankton experience. This study focused on factors that had direct
550 influence on C:N:P, we then chose to forgo using co-stressors of nutrients or the use of iron
551 stress. Along with direct influence, these samples match one to one with the POM samples
552 collected on the cruises.

553 It was determined through the use of GAM, that nutricline depth, phosphorus ~~gene~~
554 index stress, and temperature were the main drivers in the variability of C:N:P. These finding are
555 similar to those of a global synthesis that determined nutricline and gene index were the
556 dominant drivers of C:N:P variability within the tropical and subtropical regions (Tanioka et al.,
557 2022). While their pole-wards assessment determined that temperature was the dominant driver,
558 the samples used in this study fall primarily within tropical/ subtropical bounds (49 of 877
559 samples are outside of this range). C:P and N:P generally agreed with this global model
560 assessment, but C:N temperature had a smaller influence globally than for the Atlantic Ocean.
561 With the relatively small amount of variance determined for C:N, it is possible that the northern
562 most samples had a major impact on the determination of temperatures influence, as seen with
563 Tanioka et al., 2022, in which temperature was determined to be the most significant driver for
564 the variance of C:N. With respect to the other section of the GAM analysis, the factors with a
565 more indirect relationship to C:N:P could have a significant role, especially with C:N (i.e. the
566 influence of iron stress or light availability).

567 The predicted restricted changes in seasonal values of C:N:P were able to fall in the
568 middle to lower range of the observed seasonal averages of those observed at BATS,
569 representing the fall and winter seasons better than spring and summer (Singh et al., 2015). It is
570 worth noting that while the values were able to capture the lower range, the ratios measured
571 during C13.5 closest to BATS, were lower than the measured monthly averages. Since C13.5
572 was unable to take CTD measurements, the nutricline depth from WOA might not accurately
573 represent the actual nutricline depth during the transect, leading to potential changes in the
574 predictive seasonal values. The intersection point of the two transects (~10° S) also indicates
575 minimal seasonal influence as the POM and stoichiometric values despite collection occurring in

576 ~~opposite seasons. Using the values predicted by GAM for the same parameters, there was less~~
577 ~~than a 2% difference in C:N:P between fall and spring indicating that some of the assumptions~~
578 ~~made with the predictors weakened the sensitivity of the model. Without this sensitivity, the N~~
579 ~~and P limitation are assessed based on genomic changes and adaptation in *Prochlorococcus*~~
580 ~~populations (Ustiek et al., 2021). While additional genomic information can be added in the~~
581 ~~future, *Prochlorococcus* provides a starting point, as it is the most abundant and the majority of~~
582 ~~biomass for phytoplankton in the central Atlantic Ocean (Fig. S4) (Maranon et al., 2000;~~
583 ~~Zwirgmaier et al., 2007). Beyond the central Atlantic Ocean, *Prochlorococcus* is still found to~~
584 ~~be the most numerically abundant phytoplankton in the Eastern Sub-Polar regions, but biomass~~
585 ~~of other phytoplankton, with *Synechococcus* and Pico-Eukaryotes are having a larger~~
586 ~~contribution. The predicted restricted changes in seasonal values of C:N:P fall within the range~~
587 ~~of those observed at BATS, where seasonal shifts in stoichiometry were similarly weak (Singh et~~
588 ~~al., 2015). The intersection point of the two transects (~10°S) also indicates minimal seasonal~~
589 ~~influence as the POM and stoichiometric values are similar despite collection in opposite~~
590 ~~seasons. While there is a temporal difference in sampling, predictive modeling suggests that the~~
591 ~~observed biogeography of C:N:P is stable in most of the central Atlantic Ocean, albeit with~~
592 ~~several exceptions. In summary, we detect clear meridional, hemisphere, and zonal gradients in~~
593 ~~elemental stoichiometry that corresponds to changes in nutrient supply and ~~stress/limitation~~ type,~~
594 ~~but additional factors may ~~also provide a significant influence on~~ affect regional shifts in C:N:P~~
595 ~~across the Atlantic Ocean.~~

596 Our ~~POM concentration and elemental ratio~~ observations from the Atlantic Ocean have
597 implications for predicting future changes to the ocean carbon cycle. Recent models have
598 suggested that C:N:P variability can ‘buffer’ the effects of stratification and reduced nutrient
599 supply on primary productivity and carbon sequestration (Kwon et al., 2022, Tanioka and
600 Matsumoto, 2017). Such models of C:N:P variability have so far been tied to ~~the~~ surface
601 ~~phosphorus-phosphate~~ concentrations (Galbraith and Martiny, 2015). However, our observations
602 from the Atlantic Ocean indicate that subtle shifts between ~~nitrogen~~N and ~~phosphorus~~P
603 ~~limitation~~stress can have additional impacts on the elemental stoichiometry. ~~The dust deposition~~
604 ~~stimulation of N₂-fixation~~ in the North Atlantic Ocean is likely responsible for part of the shift
605 in nutrient stress type. ~~The~~is hemispheric variability ~~of nutrient stress~~ suggests an additional
606 role of iron supply in regulating C:N:P. Thus, climate change may alter future patterns of C:N:P
607 as the perturbation of air-sea dynamics can modulate the strengths of boundary currents, the
608 slope of a westward nutricline (Kelly et al., 2010), or the aeolian deposition of iron
609 (Krishnamurthy et al., 2010). Such shifts in C:N:P could, in turn, have large impacts on global
610 nitrogen fixation, primary production, or carbon sequestration.

612 **Conflict of Interest**

613 The authors declare no conflicts of interest relevant to this study.

614 **Acknowledgments**

616 We thank the Global Oceans Ship-Based Hydrographic Investigations Program (GO-SHIP) and
617 the Atlantic Meridional Transect Programme for facilitating this project. We extend a special
618 thanks to Andrew Rees, Glen Tarren, and the crew of the RSS *James Clark* and Leticia Barbero
619 and the crew of the *R/V Roger Revelle*. This research was funded by the National Science
620 Foundation (OCE-1848576 and 1948842 to ACM), NASA (80NSSC21K1654 to ACM), NOAA
621 (101813 Z7554214 to ACM), and Simons Postdoctoral Fellowship in Marine Microbial Ecology

Formatted: Indent: First line: 0.5"

Formatted: Font: (Default) Tahoma

Formatted: Font: (Default) Tahoma

Formatted: Font: (Default) Tahoma

622 (724483 to TT). The PML AMT is funded by the UK Natural Environment Research Council
623 through its National Capability Long-term Single Centre Science Program, Climate Linked
624 Atlantic Sector Science (grant number NE/R015953/1). This study contributes to the
625 international IMBeR project and is AMT contribution number XXX (number pending).

626

627 **Data availability statement**

628 The AMT data set presented here is publicly hosted by the British Oceanographic Data Centre
629 (<https://doi.org/10.5285/b5900384-89f0-3a38-e053-6c86abc0409d>). Hydrographic data from the
630 AMT28 transect are available (<https://cchdo.ucsd.edu/cruise/74JC20180923>). The particulate
631 organic matter data from the C13.5 transect are available here
632 (<https://www.bco-dmo.org/dataset/868908>). Hydrographic data from C13.5 data are available
633 (<https://cchdo.ucsd.edu/cruise/33RO20200321>). Nutricline depth for C13.5 is calculated from
634 gridded annual mean nitrate data from World Ocean Atlas 2018
635 (<https://www.ncei.noaa.gov/data/oceans/woa/WOA18/DATA/>).

636

637 **References**

638 Babiker, I. S., Mohamed, M. A. A., Komaki, K., Ohta, K., and Kato, K.: Temporal Variations in
639 the Dissolved Nutrient Stocks in the Surface Water of the Western North Atlantic Ocean, *Journal*
640 *of Oceanography*, 60, 553–562, <https://doi.org/10.1023/B:JOCE.0000038348.66907.db>, 2004.

641 Browning, T. J. and Moore, C. M.: Global analysis of ocean phytoplankton nutrient limitation
642 reveals high prevalence of co-limitation, *Nat Commun*, 14, 5014,
643 <https://doi.org/10.1038/s41467-023-40774-0>, 2023.

644 Capone, D. G.: An iron curtain in the Atlantic Ocean forms a biogeochemical divide,
645 *Proceedings of the National Academy of Sciences*, 111, 1231–1232,
646 <https://doi.org/10.1073/pnas.1322568111>, 2014.

647 Cavender-Bares, K. K., Karl, D. M., and Chisholm, S. W.: Nutrient gradients in the western
648 North Atlantic Ocean: Relationship to microbial community structure and comparison to patterns
649 in the Pacific Ocean, *Deep Sea Research Part I: Oceanographic Research Papers*, 48, 2373–2395,
650 [https://doi.org/10.1016/S0967-0637\(01\)00027-9](https://doi.org/10.1016/S0967-0637(01)00027-9), 2001.

651 Cermeño, P., Dutkiewicz, S., Harris, R. P., Follows, M., Schofield, O., and Falkowski, P. G.: The
652 role of nutricline depth in regulating the ocean carbon cycle, *Proceedings of the National*
653 *Academy of Sciences*, 105, 20344–20349, <https://doi.org/10.1073/pnas.0811302106>, 2008.

654 Clayton, S., Alexander, H., Graff, J. R., Poulton, N. J., Thompson, L. R., Benway, H., Boss, E.,
655 and Martiny, A.: Bio-GO-SHIP: The Time Is Right to Establish Global Repeat Sections of Ocean
656 Biology, *Frontiers in Marine Science*, 8, <https://doi.org/10.3389/fmars.2021.767443>, 2022.

657 Cotner, J., Ammerman, J., Peele, E., and Bentzen, E.: Phosphorus-limited bacterioplankton
658 growth in the Sargasso Sea, *Aquatic Microbial Ecology*, 13, 141–149,
659 <https://doi.org/10.3354/ame013141>, 1997.

660 Ducklow, H. and Dickson, A.: Shipboard sampling procedures, 1994.

Formatted: Font: (Default) Tahoma

Formatted: Font: Times New Roman

Formatted: Font: Times New Roman

Formatted: Font: Times New Roman

Formatted: Font: Times New Roman

Formatted: Font: Times New Roman

661 Galbraith, E. D. and Martiny, A. C.: A simple nutrient-dependence mechanism for predicting the
662 stoichiometry of marine ecosystems, *Proceedings of the National Academy of Sciences*, 112,
663 8199–8204, <https://doi.org/10.1073/pnas.1423917112>, 2015.

664 Garcia, C. A., Baer, S. E., Garcia, N. S., Rauschenberg, S., Twining, B. S., Lomas, M. W., and
665 Martiny, A. C.: Nutrient supply controls particulate elemental concentrations and ratios in the
666 low latitude eastern Indian Ocean, *Nature Communications*, 9, 4868,
667 <https://doi.org/10.1038/s41467-018-06892-w>, 2018.

668 Garcia, C. A., Hagstrom, G. I., Larkin, A. A., Ustick, L. J., Levin, S. A., Lomas, M. W., and
669 Martiny, A. C.: Linking regional shifts in microbial genome adaptation with surface ocean
670 biogeochemistry, *Philosophical Transactions of the Royal Society B: Biological Sciences*, 375,
671 20190254, <https://doi.org/10.1098/rstb.2019.0254>, 2020.

672 Isles, P. D. F.: The misuse of ratios in ecological stoichiometry, *Ecology*, 0, 1–7,
673 <https://doi.org/10.1002/ecy.3153>, 2020.

674 Kelly, K. A., Small, R. J., Samelson, R. M., Qiu, B., Joyce, T. M., Kwon, Y. O., and Cronin, M.
675 F.: Western boundary currents and frontal air-sea interaction: Gulf stream and Kuroshio
676 Extension, *Journal of Climate*, 23, 5644–5667, <https://doi.org/10.1175/2010JCLI3346.1>, 2010.

677 Kremling, K. and Streu, P.: Saharan dust influenced trace element fluxes in deep North Atlantic
678 subtropical waters, *Deep Sea Research Part I: Oceanographic Research Papers*, 40, 1155–1168,
679 [https://doi.org/10.1016/0967-0637\(93\)90131-L](https://doi.org/10.1016/0967-0637(93)90131-L), 1993.

680 Krishnamurthy, A., Moore, J. K., Mahowald, N., Luo, C., and Zender, C. S.: Impacts of
681 atmospheric nutrient inputs on marine biogeochemistry, *Journal of Geophysical Research*, 115,
682 G01006, <https://doi.org/10.1029/2009JG001115>, 2010.

683 Lee, J. A., Garcia, C. A., Larkin, A. A., Carter, B. R., and Martiny, A. C.: Linking a Latitudinal
684 Gradient in Ocean Hydrography and Elemental Stoichiometry in the Eastern Pacific Ocean,
685 *Global Biogeochemical Cycles*, 35, <https://doi.org/10.1029/2020GB006622>, 2021.

686 Lomas, M. W., Burke, A. L., Lomas, D. A., Bell, D. W., Shen, C., Dyhrman, S. T., and
687 Ammerman, J. W.: Sargasso Sea phosphorus biogeochemistry: An important role for dissolved
688 organic phosphorus (DOP), *Biogeosciences*, 7, 695–710, <https://doi.org/10.5194/bg-7-695-2010>,
689 2010.

690 Lomas, M. W., Bates, N. R., Johnson, R. J., Steinberg, D. K., and Tanioka, T.: Adaptive carbon
691 export response to warming in the Sargasso Sea, *Nature Communications*, 13, 1211,
692 <https://doi.org/10.1038/s41467-022-28842-3>, 2022.

693 Löscher, C. R., Mohr, W., Bange, H. W., and Canfield, D. E.: No nitrogen fixation in the Bay of
694 Bengal?, *Biogeosciences*, 17, 851–864, <https://doi.org/10.5194/bg-17-851-2020>, 2020.

695 Mahowald, N. M., Baker, A. R., Bergametti, G., Brooks, N., Duce, R. A., Jickells, T. D.,
696 Kubilay, N., Prospero, J. M., and Tegen, I.: Atmospheric global dust cycle and iron inputs to the
697 ocean, *Global Biogeochemical Cycles*, 19, <https://doi.org/10.1029/2004GB002402>, 2005.

698 Marañón, E., Holligan, P. M., Varela, M., Mouriño, B., and Bale, A. J.: Basin-scale variability of
699 phytoplankton biomass, production and growth in the Atlantic Ocean, *Deep Sea Research Part I:*
700 *Oceanographic Research Papers*, 47, 825–857, [https://doi.org/10.1016/S0967-0637\(99\)00087-4](https://doi.org/10.1016/S0967-0637(99)00087-4),
701 2000.

702 Martiny, A. C., Vrugt, J. A., Primeau, F. W., and Lomas, M. W.: Regional variation in the
703 particulate organic carbon to nitrogen ratio in the surface ocean, *Global Biogeochemical Cycles*,
704 27, 723–731, <https://doi.org/10.1002/gbc.20061>, 2013a.

705 Martiny, A. C., Pham, C. T. A., Primeau, F. W., Vrugt, J. A., Moore, J. K., Levin, S. A., and
706 Lomas, M. W.: Strong latitudinal patterns in the elemental ratios of marine plankton and organic
707 matter, *Nature Geoscience*, 6, 279–283, <https://doi.org/10.1038/ngeo1757>, 2013b.

708 Martiny, A. C., Lomas, M. W., Fu, W., Boyd, P. W., Chen, Y. L., Cutter, G. A., Ellwood, M. J.,
709 Furuya, K., Hashihama, F., Kanda, J., Karl, D. M., Kodama, T., Li, Q. P., Ma, J., Moutin, T.,
710 Woodward, E. M. S., and Moore, J. K.: Biogeochemical controls of surface ocean phosphate,
711 *Science Advances*, 5, eaax0341, <https://doi.org/10.1126/sciadv.aax0341>, 2019.

712 Mather, R. L., Reynolds, S. E., Wolff, G. A., Williams, R. G., Torres-Valdes, S., Woodward, E.
713 M. S., Landolfi, A., Pan, X., Sanders, R., and Achterberg, E. P.: Phosphorus cycling in the North
714 and South Atlantic Ocean subtropical gyres, *Nature Geoscience*, 1, 439–443,
715 <https://doi.org/10.1038/ngeo232>, 2008.

716 Michaels, A. F. and Knap, A. H.: Overview of the U.S. JGOFS Bermuda Atlantic Time-series
717 Study and the Hydrostation S program, *Deep Sea Research Part II: Topical Studies in*
718 *Oceanography*, 43, 157–198, [https://doi.org/10.1016/0967-0645\(96\)00004-5](https://doi.org/10.1016/0967-0645(96)00004-5), 1996.

719 Michaels, A. F., Knap, A. H., Dow, R. L., Gundersen, K., Johnson, R. J., Sorensen, J., Close, A.,
720 Knauer, G. A., Lohrenz, S. E., Asper, V. A., Tuel, M., and Bidigare, R.: Seasonal patterns of
721 ocean biogeochemistry at the U.S. JGOFS Bermuda Atlantic time-series study site, *Deep Sea*
722 *Research Part I: Oceanographic Research Papers*, 41, 1013–1038, [https://doi.org/10.1016/0967-](https://doi.org/10.1016/0967-0637(94)90016-7)
723 [0637\(94\)90016-7](https://doi.org/10.1016/0967-0637(94)90016-7), 1994.

724 Mills, M. M., Ridame, C., Davey, M., La Roche, J., and Geider, R. J.: Iron and phosphorus co-
725 limit nitrogen fixation in the eastern tropical North Atlantic, *Nature*, 429, 292–294,
726 <https://doi.org/10.1038/nature02550>, 2004.

727 Moreno, A. R., Larkin, A. A., Lee, J. A., Gerace, S. D., Tarran, G. A., and Martiny, A. C.:
728 Regulation of the Respiration Quotient Across Ocean Basins, *AGU Advances*, 3,
729 e2022AV000679, <https://doi.org/10.1029/2022AV000679>, 2022.

730 Neuer, S., Torres-Padrón, M. E., Gelado-Caballero, M. D., Rueda, M. J., Hernández-Brito, J.,
731 Davenport, R., and Wefer, G.: Dust deposition pulses to the eastern subtropical North Atlantic
732 gyre: Does ocean’s biogeochemistry respond?, *Global Biogeochemical Cycles*, 18, n/a-n/a,
733 <https://doi.org/10.1029/2004GB002228>, 2004.

734 R Core Team: R: A Language and Environment for Statistical Computing, 2021.

735 Schlitzer, R.: Ocean Data View, 2019.

736 Schlosser, C., Klar, J. K., Wake, B. D., Snow, J. T., Honey, D. J., Woodward, E. M. S., Lohan,
737 M. C., Achterberg, E. P., and Mark Moore, C.: Seasonal ITCZ migration dynamically controls
738 the location of the (sub)tropical Atlantic biogeochemical divide, *Proceedings of the National*
739 *Academy of Sciences of the United States of America*, 111, 1438–1442,
740 <https://doi.org/10.1073/pnas.1318670111>, 2014.

741 Singh, A., Baer, S. E., Riebesell, U., Martiny, A. C., and Lomas, M. W.: C : N : P stoichiometry
742 at the Bermuda Atlantic Time-series Study station in the North Atlantic Ocean, *Biogeosciences*,
743 12, 6389–6403, <https://doi.org/10.5194/bg-12-6389-2015>, 2015.

744 Steinberg, D. K., Carlson, C. A., Bates, N. R., Johnson, R. J., Michaels, A. F., and Knap, A. H.:
745 Overview of the US JGOFS Bermuda Atlantic Time-series Study (BATS): a decade-scale look at
746 ocean biology and biogeochemistry, *Deep Sea Research Part II: Topical Studies in*
747 *Oceanography*, 48, 1405–1447, [https://doi.org/10.1016/S0967-0645\(00\)00148-X](https://doi.org/10.1016/S0967-0645(00)00148-X), 2001.

748 Swift, J.: CTD data from Cruise 74JC20180923, <https://doi.org/10.7942/C2D08M>, 2019.

749 Tanioka, T. and Matsumoto, K.: Buffering of Ocean Export Production by Flexible Elemental
750 Stoichiometry of Particulate Organic Matter, *Global Biogeochemical Cycles*, 31, 1528–1542,
751 <https://doi.org/10.1002/2017GB005670>, 2017.

752 Tanioka, T. and Matsumoto, K.: A meta-analysis on environmental drivers of marine
753 phytoplankton, *Biogeosciences*, 17, 2939–2954, <https://doi.org/10.5194/bg-17-2939-2020>, 2020.

754 Tanioka, T., Garcia, C. A., Larkin, A. A., Garcia, N. S., Fagan, A. J., and Martiny, A. C.: Global
755 patterns and predictors of C:N:P in marine ecosystems, *Commun Earth Environ*, 3, 1–9,
756 <https://doi.org/10.1038/s43247-022-00603-6>, 2022.

757 Ussher, S. J., Achterberg, E. P., Powell, C., Baker, A. R., Jickells, T. D., Torres, R., and
758 Worsfold, P. J.: Impact of atmospheric deposition on the contrasting iron biogeochemistry of the
759 North and South Atlantic Ocean, *Global Biogeochemical Cycles*, 27, 1096–1107,
760 <https://doi.org/10.1002/gbc.20056>, 2013.

761 Ustick, L. J., Larkin, A. A., Garcia, C. A., Garcia, N. S., Brock, M. L., Lee, J. A., Wiseman, N.
762 A., Moore, J. K., and Martiny, A. C.: Metagenomic analysis reveals global-scale patterns of
763 ocean nutrient limitation, *Science*, 372, 287–291, <https://doi.org/10.1126/science.abe6301>, 2021.

764 Utermöhl, H.: Zur Vervollkommnung der quantitativen Phytoplankton-Methodik, *Internationale*
765 *Vereinigung für Theoretische und Angewandte Limnologie: Mitteilungen*, 9, 1–38,
766 <https://doi.org/10.1080/05384680.1958.11904091>, 1958.

767 Wang, W.-L., Moore, J. K., Martiny, A. C., and Primeau, F. W.: Convergent estimates of marine
768 nitrogen fixation, *Nature*, 566, 205–211, <https://doi.org/10.1038/s41586-019-0911-2>, 2019.

769 Weber, T. S. and Deutsch, C.: Ocean nutrient ratios governed by plankton biogeography, *Nature*,
770 467, 550–554, <https://doi.org/10.1038/nature09403>, 2010.

771 Wood, S. N.: Generalized Additive Models, Chapman and Hall/CRC,
772 <https://doi.org/10.1201/9781315370279>, 2017.

773 Yvon-Durocher, G., Dossena, M., Trimmer, M., Woodward, G., and Allen, A. P.: Temperature
774 and the biogeography of algal stoichiometry, *Global Ecology and Biogeography*, 24, 562–570,
775 <https://doi.org/10.1111/geb.12280>, 2015.

776 Zwirgmaier, K., Heywood, J. L., Chamberlain, K., Woodward, E. M. S., Zubkov, M. V., and
777 Scanlan, D. J.: Basin-scale distribution patterns of picocyanobacterial lineages in the Atlantic
778 Ocean, *Environmental Microbiology*, 9, 1278–1290, [https://doi.org/10.1111/j.1462-](https://doi.org/10.1111/j.1462-2920.2007.01246.x)
779 [2920.2007.01246.x](https://doi.org/10.1111/j.1462-2920.2007.01246.x), 2007.

780 ~~Zwirgmaier, K., Heywood, J. L., Chamberlain, K., Woodward, E. M. S., Zubkov, M. V., &~~
781 ~~——— Scanlan, D. J. (2007). Basin-scale distribution patterns of picocyanobacterial lineages in~~
782 ~~the Atlantic Ocean. *Environmental Microbiology*, 9(5), 1278–1290.~~
783 ~~<https://doi.org/10.1111/j.1462-2920.2007.01246.x>~~
784

Formatted: Widow/Orphan control, Adjust space between Latin and Asian text, Adjust space between Asian text and numbers